LTrack: A LoRa-Based Indoor Tracking System for Mobile Robots

Kang Hu , *Student Member, IEEE*, Chaojie Gu , *Member, IEEE*, and Jiming Chen , *Fellow, IEEE*

Abstract—The robot's mobility and intelligence have expanded its application in recent years. Specifically, indoor tracking is a fundamental function of public service robots in nursing homes, hospitals, and warehouses. Existing vision-based tracking requires visual information, which may be unavailable and introduce privacy issues in practical deployment. To this end, in this paper, we propose **LTrack**, a long-range tracking system based on LoRa, an emerging low-power wide-area networking (LPWAN) technology, with a single transceiver pair. Note that commodity LoRa devices cannot estimate the angle of arrival (AoA) of signals due to hardware limitations. We design a virtual circular antenna array in the mobile rotating anchor via a lightweight hardware modification to multiplex the only RF channel in the low-cost LoRa device. The difference of time of flight (TDoF) measured in the circular antenna array is fused with the rotating orientation to estimate the target AoA. We also redesign and optimize the primitive LoRa ranging engine based on systematic analysis. Further, we present a real-time mobile target tracking algorithm based on the Doppler frequency shift to combat the uncertainty introduced by the target movement. We have developed the prototype of **LTrack**, which consists of a mobile rotating anchor, a LoRa tag, and a commercial robot. The system is evaluated in both LOS and NOLS indoor scenarios. Experiments show that **LTrack** supports robust tracking with a median error of 0.12 m and 0.45 m in a 137 m^2 lab space and a 600 m^2 corridor, respectively.

Index Terms—Indoor tracking, mobile robots, LoRa, AoA estimation.

I. INTRODUCTION

THE last decade witnessed the boost in sales value of service robots. The market size of service robots was 12.88 billion US$ in 2019 and is estimated to reach 41.49 billion US$ by 2027 [1]. The service robot compensates for the lack of human resources with its long working hours and high efficiency. They have been widely deployed in nursing homes, warehouses, airports, and hospitals. During the current COVID-19 pandemic, the service robot helps reduce direct human-to-human contacts and thus cuts the possible transmission route. Unlike the traditional service robots that are stationary, modern service robots move around to extend their working area [2], [3]. Specifically,

tracking is an essential system function of mobile robots to follow or monitor a target in the navigation, following, and guiding services. The mobile service robot first gets the relative location to the target and then plans the tracking trajectory. For example, medical robots follow and assist doctors or nurses closely in hospitals where the GPS signal is weak in such indoor environments due to signal attenuation. Thus, it is desirable to design indoor tracking approaches for mobile robots.

Researchers have proposed various approaches to implement indoor tracking functions for mobile robots, either vision-based, including RGB camera [4], visual sensing [5], or RF-based, including Wi-Fi [6], Bluetooth [7], and UWB [8]. While the vision-based approaches achieve sub-meter accuracy, they may introduce privacy issues as the consumer face image is collected for identification [9]. Moreover, most vision-based tracking approaches utilize camera images in the local sight areas, which prevents the utility in large areas and many invisible emergencies. In contrast, the RF-based approaches collect the wireless signal and preserve users' privacy. However, most RF-based approaches are not applicable in complex indoor environments or have limited coverage due to signal attenuation. These systems usually require prior knowledge by ad-hoc profiling or setting more infrastructures to improve accuracy or extend coverage [10].

Low-power wide-area networking (LPWAN) is an emerging wireless network paradigm that aims to provide long-range ubiquitous connectivity to the Internet of Things (IoT) devices [11]. LoRa is a representative LPWAN technology, which operates on license-free industrial, scientific, and medical (ISM) bands using low-cost devices. LoRa is resilient to noise and has a long-range communication capability due to its Chirp Spreading Spectrum (CSS) modulation scheme. Because of these advantages, recently, there has been a trend of exploiting LoRa in indoor applications, e.g., sensing [12], [13] and localization [14]. It is interesting to investigate the feasibility of implementing a LoRa-based tracking system. A straightforward idea is that users can keep performing multilateration to enable tracking functions. However, the timestamps in current commercial off-the-shelf (COTS) LoRa devices do not have sufficient resolution [15]. The users need extra efforts and set additional software-defined radios (SDRs) to upgrade existing infrastructure and improve the accuracy [16]. Another approach is fusing the time difference of arrival (TDoA) and angle of arrival (AoA) to track the target [17]. Unfortunately, the standard LoRa does not support AoA estimation due to hardware limitations. Some recent studies propose to use MIMO devices

to enable AoA estimation at the anchor side [18]. However, these designs rely on expensive SDRs like Universal Software Radio Peripherals (USRPs), which face the same cost issue as the multilateration approach has [19]. Moreover, users often set a high sampling rate of the SDRs device to increase accuracy, generating large data files and taking lots of time to process.

In this paper, we present LTrack, a LoRa-based indoor tracking system with only a single transceiver pair, which supports *in situ* deployment and provides high tracking accuracy (∼0.45 m). LTrack deploys an *anchor* (gateway) on a mobile robot and attaches one or multiple *tags* (end devices) to the tracking targets. The robot detects the environments to avoid obstacles via a Lidar and an illumination-insensitive depth camera, which can protect privacy [20]. Note that LTrack is designed for mobile robots, which means that it does not require any prior infrastructure when the robot is deployed. At run time, the anchor tracks the target and navigates the robot by communicating with the tag using LoRa. Specifically, we select 2.4 GHz LoRa to prototype LTrack because of its ranging engine, which is not available in sub-1 GHz LoRa chips. With a lightweight and low-cost modification based on an SX1280 chip, we prototype the LTrack anchor (costs 20 US$) that is 250× cheaper than a USRP. The LTrack tag can be any SX1280-based end device.

The design of LTrack is challenging due to three practical factors. The first challenge is the unavailability of AoA estimation in COTS LoRa transceivers. Channel state information (CSI) provides channel properties of a communication link, which can be used for AoA estimation. Different from other RF technologies like Wi-Fi, CSI is unavailable in COTS LoRa devices. To empower the COTS LoRa device with AoA estimation, we embed an RF switch to allow the LoRa chip to access external antennas for AoA estimation (see Section IV-A1). The RF chain is multiplexed in a time-division fashion. Thus, the anchor can estimate the AoA with ranging measurements from the external antennas. However, such an approach is coarse-grained due to the error introduced by the waiting time between ToF estimations. Notice that 2.4 GHz LoRa hops among 40 subchannels pseudo-randomly to achieve a stable estimation of the time of flight (ToF). As a result, a ToF estimation lasts 160 ms, which contains a round-trip time of 40 frames. The LoRa chip has to finish all ToF estimations at the first antenna before switching to another. During this period, the surrounding environment may change, and the target may move, which degrades the AoA estimation accuracy. To address this issue, we design a new ranging pipeline for LTrack (see Section IV-A2) to minimize waiting time in the antenna array and thus improve the accuracy.

The second challenge is the antenna array self-interference. The antennas in a static antenna array block each other and thus cause blind areas. Adding more antennas to reduce blind areas increases the implementation cost and complexity. Inspired by Synthetic Aperture Radar (SAR) [21], LTrack uses a circular antenna array to emulate a "virtual array" to eliminate blind areas. The circular antenna array rotates and takes snapshots of received signals at different spatial locations. Since the rotation speed and angle can be measured, we further design an algorithm (see Section IV-B) that can jointly estimate the target location according to snapshots.

Another challenge is the impact of target movement. Although we can increase the estimation frequency at the *anchor* side, the impact of target movement is unavoidable in a tracking system. LTrack exploits the Doppler frequency shift to estimate the target movement (see Section IV-C). Specifically, we analyze the target movement model and design a lightweight frequency estimation algorithm. With such an algorithm, LTrack further improves its real-time tracking performance.

Scope and Limitations: We emphasize that LTrack: 1) Considers tracking objects in a 2-D space. 2) Is designed for mobile robot, AGV, and IGV systems. We reuse the robot to implement the tracking, and thus, the additional cost is negligible. 3) Achieves real-time tracking but is affected by the moving speed of the target (analysis in Section IV-C and discussion in Section VI). Yet, LTrack remains broadly applicable for most indoor tracking applications.

Evaluation and Results: The LTrack prototype includes a LoRa anchor (gateway) and a LoRa tag (end device). We deploy the anchor on a mobile robot and perform evaluations. Our results show that:

1) Compared with the primitive LoRa ranging engine, LTrack improves the ranging TDoF accuracy by 302%.
2) LTrack respectively achieves median errors of $4.5°$ and $5.72°$ in LOS and NLOS AoA estimations at 50 m.
3) LTrack can track a moving object with a speed up to 0.5 m/s in real-time with a 0.45 m median error.

Contributions: The contributions of this paper include:

1) We for the first time demonstrate the feasibility of enabling AoA estimation on the COTS LoRa chip with one RF channel and optimize the ranging protocol to improve the accuracy.
2) We design a new LoRa anchor with a circular antenna array to achieve fine-grained AoA estimation and eliminate the blind areas.
3) We build the motion model of a moving object and propose an algorithm to track moving objects via real-time velocity estimation.
4) We prototype the proposed tracking system and conduct experiments to evaluate its performance in complex indoor environments.

The rest of this paper is organized as follows. Section II introduces the background. Section III overviews the system. Section IV presents the details on the system design. Section V describes the system implementation. Section VI shows the simulation and experiment results. Section VII reviews related work and Section VIII concludes this paper.

II. BACKGROUND

In this section, we first present LoRa primer and its ranging engine. Then, we introduce the principle of AoA estimation.

A. LoRa Primer and Its Ranging Engine

LoRa runs on the ISM bands and supports long-range communication with low-power consumption. It is available on both sub-1 GHz (e.g., 868 MHz in EU) and 2.4 GHz bands. LoRa's CSS modulation techniques empower its large network

coverage, i.e., 1-5 km in urban areas and up to 25 km in rural areas. Compared with LoRa radios operating on sub-1 GHz bands (i.e., 433 MHz, 868 MHz, 915 MHz), 2.4 GHz LoRa has a wider bandwidth [16], which is more applicable for ranging tasks. 2.4 GHz LoRa has 8 spreading factors (SFs) starting from SF5 to SF12, and a variable bandwidth (BW) range of 0.2 MHz-1.6 MHz. At run time, 2.4 GHz LoRa hops over its 40 subchannels to avoid interference from other radios. The bandwidth of each subchannel is 2 MHz. As a result, the 2.4 GHz LoRa's bandwidth ranges from 2.40 GHz to 2.48 GHz.

Different from the sub-1 GHz LoRa chip, the 2.4 GHz LoRa chip defines a ranging engine by measuring the ToF between two nodes. Specifically, the anchor node sends a ranging packet consisting of preambles, a target address, and ranging symbols for the detection, identification, and synchronization, respectively. In the meanwhile, it starts a clock counter for timing. When the target node receives the packet, it immediately replies to the anchor node with a responding ranging packet. Upon receiving the response from the target node, the anchor node gets the counter number and calculates the result with a filter (e.g., median filter). As there are 40 subchannels in 2.4 GHz LoRa, the ranging engine keeps hopping and performing ranging on each subchannel. The ranging resolution is limited in most narrowband communications. However, the CSS adopts wideband linear frequency modulated chirp pulses to send the signal. As the spectrum is extensively spread, the distance resolution of the LoRa ranging engine, which is corresponding to one least significant bit (LSB), is given by

$$D_{LSB} = \frac{c}{2^{12}BW}, \qquad (1)$$

where BW is the bandwidth in Hz and c is the speed of light. Further, the distance d can be calculated by

$$d = 0.5 D_{LSB} N, \qquad (2)$$

where N is the clock counter number.

Note that the resolution is different from the accuracy. In the noise-limited RF ToF ranging case, the ranging performance is affected by the bandwidth, spreading factor, signal-to-noise ratio (SNR), and the number of ranging symbols. According to the Cramér-Rao bound for the accuracy of the LoRa unbiased estimator, the ToF variance is bounded by

$$\sigma_{tof}^2 = \frac{1}{8\pi^2 SNR\sqrt{M}BW2^{SF}}, \qquad (3)$$

where M is the number of ranging symbols, and SF is the spreading factor. For ranging operations, the use of SF11 and SF12 is not permitted in the chipset. Similarly, the bandwidth configuration for ranging operations is restricted to 406.25 kHz, 812.5 kHz, and 1625 kHz.

B. AoA Estimation

The most common approach to estimate AoA is exploiting phase information of signals (e.g., Wi-Fi, Bluetooth) [22]. The anchor leverages an array of antennas at different locations to receive the packet sent by the transceiver simultaneously. The antennas in the array are separated by a fixed distance to reduce
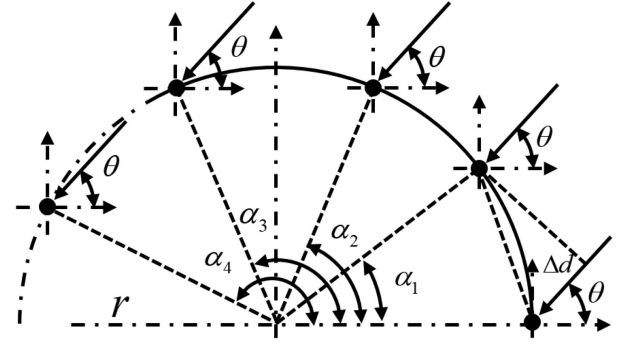

Fig. 1.   The structure of a circular antenna array. Each antenna captures the signals for the AoA estimation. All of the antennas are arranged in a circle.
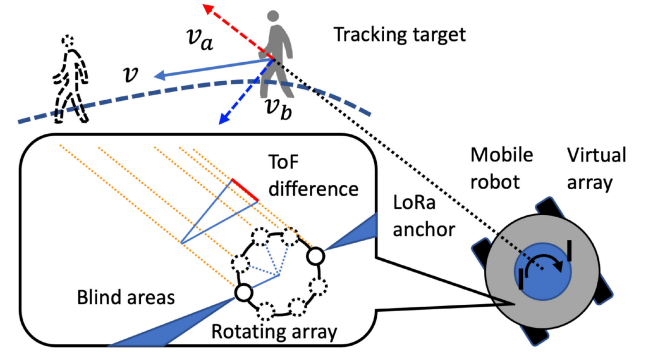

Fig. 2.   Overview of the tracking system.

the coupling, e.g., 0.5 to 1 time of the wavelength. All antennas receive the signals from the target node and extract the phase to estimate the AoA jointly. The signal phases retrieved from the antennas are different since the antennas are at different locations. For example, in a circular array illustrated in Fig. 1, the AoA θ is estimated by a steering vector $\mathbf{c}(\theta)$, which can be expressed by

$$\mathbf{c}(\theta) = \begin{bmatrix} e^{2\pi j \frac{r\cos(\theta - \alpha_1)}{\lambda}} \\ e^{2\pi j \frac{r\cos(\theta - \alpha_2)}{\lambda}} \\ \ldots \\ e^{2\pi j \frac{r\cos(\theta - \alpha_n)}{\lambda}} \end{bmatrix}, \qquad (4)$$

where $\alpha_i, i = 1, \ldots, n$, λ, and r are antenna orientation, signal wavelength, and array radius, respectively [23]. Note that most MIMO systems and Wi-Fi routers have built-in CSI analyzers for retrieving phase information [6], [23]. However, built-in CSI analyzers are missing in most low-power and low-cost devices.

III. SYSTEM OVERVIEW

This section introduces an overview of LTrack system and practical challenges. The primary goal of LTrack is to locate and track a target, either static or mobile, according to the received LoRa signals from an end node attached to the target. As shown in Fig. 2, LTrack's system architecture is designed as follows: The anchor sends the ranging packets via two connected antennas and collects the ranging difference. Meanwhile, the two antennas are rotated in the robot. The anchor estimates the
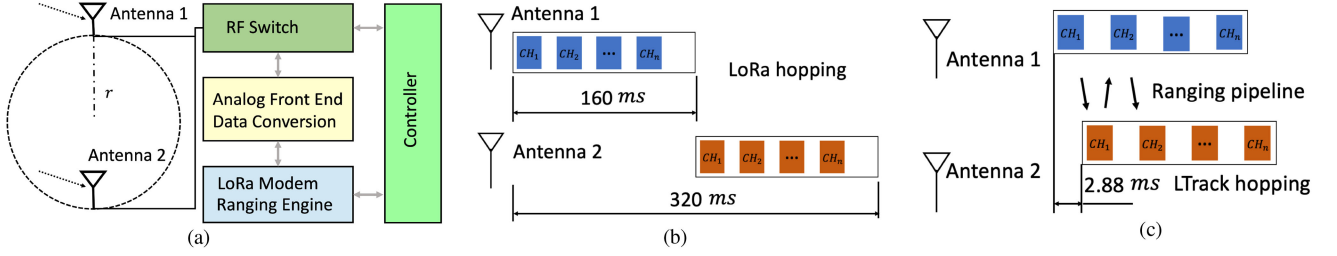
Fig. 3. We redesign the standard ranging procedure in 2.4 GHz LoRa. The antennas are selected by the controller via an RF switch, and the hopping procedure is optimized to reduce the time between TDoF estimations from two external antennas. (a) Antenna array structure. (b) Built-in hopping procedure. (c) Optimized hopping procedure.

TDoF between two antennas, the distance to the target, and the corresponding array orientation. These results are transmitted to the robot via the communication module. Further, the robot calculates the target location and schedules the path to move to this destination.

The rest of this section describes the challenges of achieving such a design.

1) Estimating the AoA: LTrack first designs a double-antenna array, which transforms the ToF estimations at two antennas into AoA. LTrack develops an antenna switching scheme that allows the LoRa chip can fully utilize its TX and RX channels simultaneously. By doing so, the LoRa chip skips the waiting time between ToF estimations and thus improves accuracy (see Section IV-A).

2) Eliminating blind areas: Next, LTrack analyzes the cause of why a two-antenna array cannot well cover a 2-D space blind area. To eliminate the blind area, LTrack emulates a virtual antenna array by rotating the double-antenna array. LTrack combines measurements of multiple virtual array pairs at different spatial locations to estimate target location (see Section IV-B).

3) Estimating target movement: LTrack then exploits the Doppler frequency shift to estimate the target movement. LTrack implements a lightweight real-time frequency estimation algorithm. By tracking the frequency shift of the received TDoF signals, LTrack further improves its tracking accuracy (see Section IV-C).

IV. SYSTEM DESIGN

In this section, we introduce our design to overcome the challenges. We first present the detail on the AoA estimation and then illustrate the method to eliminate the blind area. Finally, the target movement estimation algorithm is proposed.

A. Estimating the AoA

To estimate the AoA, we empower the COTS LoRa chip with AoA estimation capability with a lightweight hardware modification. Further, we optimize the default ranging workflow in the 2.4 GHz LoRa chip to improve the accuracy of AoA estimation.

1) AoA Estimation With an Antenna Array: As mentioned before, compared with MIMO devices, LoRa transceiver has only one RF channel for uplink and downlink transmissions, and the signal phase information is unavailable due to hardware

limitations. Therefore, it is impossible to utilize the phase difference to calculate AoA. To empower LoRa transceiver with AoA estimation capability, we propose to apply a lightweight modification on the COTS LoRa chip, as shown in Fig. 3(a). The modification requires users to add two antennas and an RF switch, which is easy to implement. The two external antennas are connected to the LoRa analog front end via the RF switch. In this way, we can exploit the difference of the ToFs received at two antennas to calculate the distance difference, denoted by Δd, from the target node to these two antennas, and further calculate the AoA, denoted by θ.

We denote the number of antennas by n, the angle between antenna i and antenna 1 (reference antenna) by α_i, and the radius of the circular antenna array by r. For antenna i and antenna 1, the distance difference, denoted by Δd_{i1}, is

$$\Delta d_{i1} = TDoF_{i1} \times c, i = 2, 3, \ldots, n. \tag{5}$$

According to Eq. 4, $\Delta \mathbf{d}(\theta)$ is a function of θ and can be expressed as:

$$\Delta \mathbf{d}(\theta) = \begin{bmatrix} 2r \sin(\frac{\alpha_2}{2}) \sin(\theta - \frac{\alpha_2}{2}) \\ 2r \sin(\frac{\alpha_3}{2}) \sin(\theta - \frac{\alpha_3}{2}) \\ \ldots \\ 2r \sin(\frac{\alpha_n}{2}) \sin(\theta - \frac{\alpha_n}{2}) \end{bmatrix}. \tag{6}$$

From a circular array with n antennas, we can obtain an accurate AoA estimation if Δd measurement is accurate. However, as illustrated in Fig. 3(b), the LoRa chip needs to process signals received at antennas one by one. In SX1280, it takes about 160 ms to finish a ranging task on 40 subchannels, and the time is doubled in the TDoF measurement. During this period, the target may move and the around environment may change, and the AoA θ can not be derived from the TDoF Δd. Thus, it is important to minimize such a waiting time.

2) Minimize Ranging Interval: We optimize the hopping process by introducing an antenna switching scheme, in which the anchor selects TX antenna between the hopping process, as shown in Fig. 3(c). Specifically, the anchor actively controls the RF switch to select the connected antenna before the transmission. When a ranging packet on the CH_1 subchannel is processed from the first antenna (antenna 1 in Fig. 3(c)), we switch to another antenna (antenna 2 in Fig. 3(c)) to transmit a ranging packet on the same subchannel, CH_1, immediately. Then, we switch back to the first antenna for ranging packet transmission on the next subchannel, i.e., CH_2. With the antenna switching
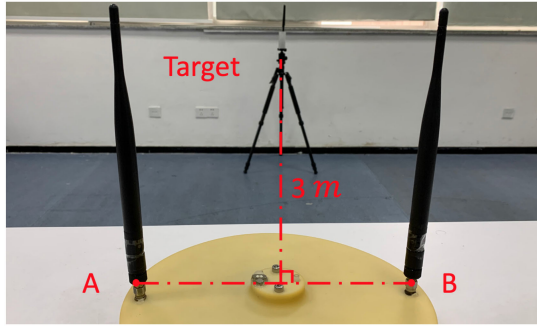
Fig. 4. The setup of the TDoF mircobenchmark. The target is put in the perpendicular bisector of the segment AB, making the ground-truth TDoF be 0.

Fig. 5. Histograms with density curve of **LTrack** and the built-in method results. In the bulit-in method, the anchor runs the standard hopping scheme.

scheme, the waiting time between two ranging operations on a subchannel decreases from 40 ranging operations time to 1 ranging operation time.

Note that an RF switch takes extra 150 ns to select the antenna. We reschedule the ranging process to reduce the interval for each ranging task. In every subchannel, the controller needs to concatenate the ranging parameters, including packet type, frequency, and bandwidth, with the original frame before transmission, increasing processing time. These parameters are usually fixed for tracking a specific target. Hence, we can prepare all the ranging packets in advance when the end device is idle. In particular, the synchronization packet selects the pseudo-random frequency hopping channels between the anchor and the target during the ranging. To this end, we move the synchronization packet generation process that was in-between the hopping process ahead. Further, the ranging packets are prepared after the system booting, reducing 13 and 17 commands in the ranging and hopping process, respectively. From our measurements, the proposed reschedule saves 0.218 ms.

After getting a ranging measurement, the LoRa ranging engine calibrates the hardware delay to output the final estimation. The hardware delay is design-specific and has been profiled in the factory, which can be taken as a constant value. Since we focus on utilizing the TDoFs for AoA estimation, the hardware uncertainty is similar in two adjacent ranging tasks and can be subtracted in the differential data. Thus, instead of performing calibration during the ranging procedure, we move the calibration at the end of AoA estimation to reduce the estimation time. From our measurements, we save 46 ms in an AoA estimation. Finally, the ranging interval is reduced from 160 ms to 2.88 ms. Hence, the impacts introduced by the target movement are mitigated a lot when calculating the TDoF (a 0.5 m/s speed leads to 0.144 cm location change).

To understand the performance gain of the proposed design quantitatively, we conduct experiments to compare the primitive LoRa ranging procedure and **LTrack** ranging pipeline regarding the TDoF estimation accuracy. As shown in Fig. 4, the target is placed at the front of the antenna array 3 m away. The mounting points of the two antennas are denoted by A and B, which are separated by 0.2 m. The target is put in the perpendicular bisector of the segment AB, making the ground-truth TDoF be 0. We use the primitive LoRa ranging procedure and **LTrack**
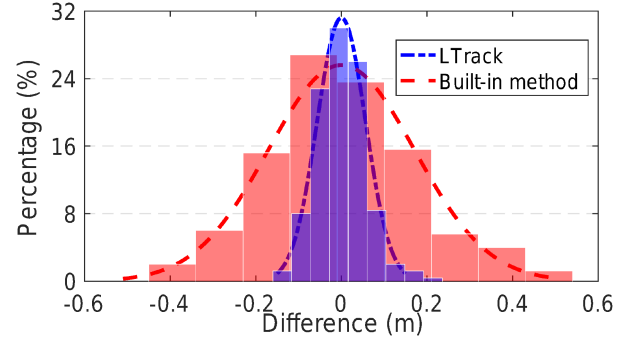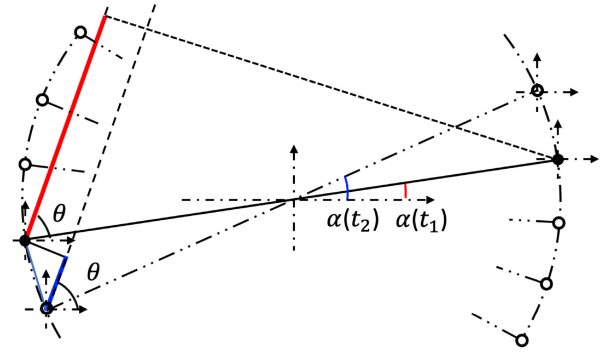

Fig. 6. The basic idea of the virtual antenna array. In rotation, the two connected antennas emulate a circular antenna array.

ranging pipeline to measure the TDoF 250 times. Fig. 5 presents the histogram of the experiment results of two pipelines. We can see that by using the built-in ranging procedure of LoRa, the values of distance difference Δd varies from -0.5 m to 0.5 m. The standard deviation is 0.171 m, which is 85.5% of the distance between antennas. Those fluctuation results in large noise for AoA estimation. The values of Δd vary from -0.2 m to 0.2 m when LTrack pipeline is used for TDoF estimation. The standard deviation is 0.057 m, which is 33% of that by using the built-in ranging procedure of LoRa. The results demonstrate that the redesigned ranging procedure is efficient to mitigate the uncertainty in TDoF estimation.

B. Eliminating the Blind Area

Although we have enabled the LoRa chip with AoA estimation capability and optimized the primitive ranging pipeline to improve accuracy, the static antenna array cannot remove the impact of the blind area. As shown in Fig. 2, in a static antenna array, the antennas block each other and thus generate the blind area. When the target is in the blind area, the AoA estimation accuracy decreases due to the blockage. To overcome this disadvantage, we design a "virtual array" based on the static antenna array proposed in Section IV-A1. As shown in Fig. 6, the "virtual array" is a circular antenna array consisting of two antennas. The circular antenna array rotates at a certain speed to emulate an antenna array of numerous antennas, and

take snapshots of received signals at different spatial locations. During the rotation, the anchor keeps sending and receiving the ranging packet, and records the orientation and speeds of the antenna array. The "virtual array" exploits the spatial diversity of the antennas to eliminate the blind area.

Specifically, the two connected antennas are driven by a DC motor in the anchor. The array orientation $\alpha(t)$ is collected via a photoelectric encoder. Since the TDoF measurements take time of once ranging when the array is rotated, the $\Delta d(t)$ needs to be synchronized with the array orientation. We assume that the first ToF_1 from antenna 1 is measured at time t_1 and the array orientation is $\alpha(t_1)$. When the second ToF_2 from antenna 2 is measured, the array is rotated to angle $\alpha(t_2)$. Therefore, the TDoF calculated from ToF_1 and ToF_2 contains the difference caused by the orientation. The difference caused by the rotation can be calculated by

$$\Delta d_r = 2r \sin\left(\frac{\alpha(t_2) - \alpha(t_1)}{2}\right) \sin\left(\theta - \frac{\alpha(t_1) + \alpha(t_2)}{2}\right). \quad (7)$$

In particular, the distance d not only contains the distance from the anchor antenna to the target antenna, but also the equivalent distance from the antenna to the chip, which includes the RF chain length and the hardware biased distance. The equivalent hardware distance difference is denoted by b. Thus, the distance difference can be synchronized by

$$\Delta d = d_2 - d_1 + b - \Delta d_r. \quad (8)$$

In the rotation, the orientations $\alpha(t)$ are recorded at the ranging time $t_1, t_2, \ldots t_n$ as $\alpha(t_1), \alpha(t_2), \ldots \alpha(t_n)$, and the responding distance difference are $\Delta d_1, \Delta d_2, \ldots \Delta d_n$. When the anchor collects an array of results, the AoA can be further estimated by

$$\min_{\theta, b} \quad h(\theta, b) = \|\widetilde{\Delta \mathbf{d}} - \Delta \mathbf{d}(\theta, b)\|, \quad (9)$$

where $\widetilde{\Delta \mathbf{d}}$ is the collected TDoF samples from the anchor. As the object function h is not a convex function, this problem is not convex. Thus, it is difficult to calculate the close-form solution. We adopt the Stochastic Gradient Descent (SGD) optimization [24] to find a solution for the AoA estimation. Specifically, we randomly select a batch comprised of a subset of measured results. The AoA θ and the bias b are initialed and then further updated in the iteration. In each calculation, we select a step size μ to update the parameters with the gradient of the object function as follows

$$\begin{bmatrix} \theta_{i+1} \\ b_{i+1} \end{bmatrix} = \begin{bmatrix} \theta_i \\ b_i \end{bmatrix} - \mu \nabla h_{t+1}([\theta_i, b_i]^{\mathrm{T}}), \quad (10)$$

where ∇h_{t+1} is the gradient function. The iteration terminates and returns the results after exceeding the maximum number of calculations or the parameters change is less than the threshold.

We conduct experiments to compare the AoA estimation accuracy of the static antenna array and the circular antenna array. The tag is placed at a set of points around the anchor, and each point is separated by 5 degrees at the distance of $3\ m$ as shown in Fig. 7. We translate the AoA estimation results into TDoF to get a better understanding and the measurement results
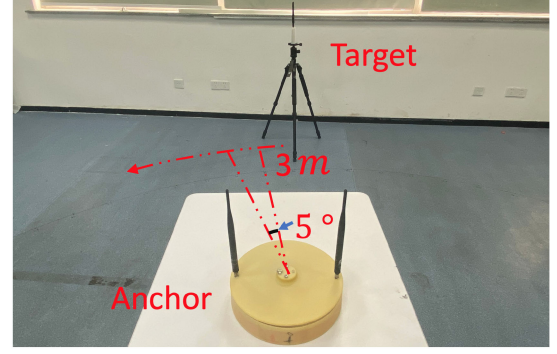

Fig. 7. The setup of the AoA estimation accuracy microbenchmark. We place the target at different locations separated by 5 degrees. The distance between the anchor and the target is 3 m.
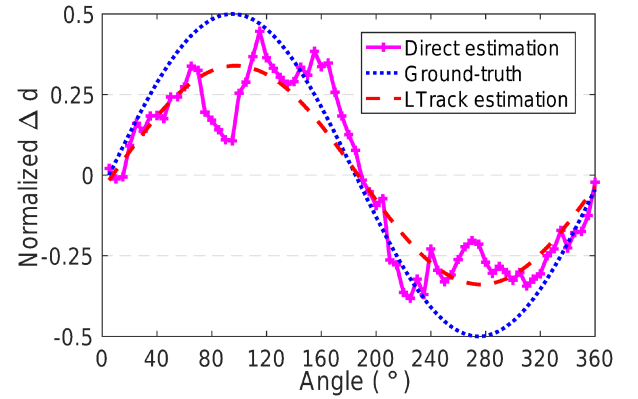

Fig. 8. To gain a better understanding, we translate the AoA into TDoF. In the blind areas, direct estimation with a static antenna array bias from the ground truth with an AoA error of more than 40 degrees.

are illustrated in Fig. 8. We can see that the error biases from the ground-truth around the 90-degree and 270-degree areas. Only a few points achieve accurate results. This is because the noise in the two periods is different and even obvious in the blind areas. The fixed antenna array causes the blind area due to the nonlinear model and the obstacles of the antenna itself. Thus, the performance is unrobust in practical environments.

C. Estimating Target Movement

Note that SAR has a fundamental assumption that the relative position between the antenna and the target device remains unchanged during the sampling procedure. In our tracking system, the target may move and change its location before the anchor finishes the estimation. Thus, the tracking performance will be degraded. To improve the tracking accuracy, we first model the target motion for moving objects. Then, we implement a real-time frequency estimation algorithm to estimate the target movement.

1) Target Motion Model: Fig. 9 illustrates the robot tracks a mobile target in a 2-D space. We can set the start point of the robot as the origin to build a coordinate system. The location of the robot at time t is denoted by $[x_r(t), y_r(t)]$. $\varphi_r(t)$ represents
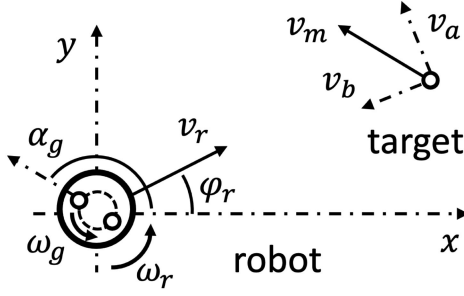
Fig. 9. The tracking model considers the tracking in a 2-D space. The anchor estimates the relative distance, angle, and velocity of the target.

the heading orientation of the robot. When the robot tracks the target, it needs to adjust its heading orientation from time to time. Thus, the line velocity and angular speed are denoted by $v_r(t)$ and $\omega_r(t)$, respectively. As the anchor is installed on the robot, its location and velocity are equal to the robot's. Note that the circular antenna array rotates at a certain speed, the orientation of the circular antenna array and its rotation speed are denoted by $\alpha_g(t)$ and $\omega_g(t)$, respectively. Similarly, the target location and velocity are denoted by $[x_m(t), y_m(t)]$ and $v_m(t)$, respectively. In particular, the anchor needs to estimate the target relative velocity, as illustrated in Fig. 2. We decompose the target's velocity v_m into tangential velocity v_a and radial velocity v_b. The radial velocity v_b to the anchor can be calculated from the ranging results. The tangential velocity v_a is proportional to the distance d and the angular velocity ω_m:

$$v_a(t) = \omega_m(t)d(t). \tag{11}$$

Note that the observed difference signal frequency ω_o in the anchor is corrected to the antenna rotation speed ω_g and the target angular speed ω_m. According to the Doppler shift model, ω_m can be calculated by

$$\omega_m(t) = \omega_g(t) - \omega_o(t). \tag{12}$$

Therefore, we can calculate the target velocity based on the observed signal frequency difference.

2) Real-Time Frequency Estimation: As the antenna array rotation frequency can be obtained from the anchor, we need to estimate the observed distance difference frequency for real-time tracking. The time-frequency features of non-stationary signals have been widely investigated in health monitoring, radar systems, *etc*. Specifically, the continuous wavelet transform (CWT) is a popular method that can calculate the time-frequency features. When the signal $\Delta d(t)$ is sampled, the time-frequency coefficients can be obtained via the CWT calculation. As the wavelet scalar is specified as positive, the negative frequency would be lost in the calculation. Thus, we select the anchor frequency that is larger than the target's velocity. Hence, the coefficients can be calculated as follows

$$[wt, f] = cwt(\Delta d(t), fs), \tag{13}$$

where wt is a matrix and every row corresponds to one scale, f is the frequencies, and fs is the sampling frequency of $\Delta d(t)$. We select the morlet wavelet as the wavelet basis function in the

transform and further extract the time-frequency features $\omega_o(t)$ via wavelet ridge detection from the coefficients $[wt, f]$.

Based on the frequency estimation, we can calculate the real-time velocity of the target. Thus, we further estimate the real-time AoA of the target via the time-frequency features instead of the motion prediction (assuming the target track in a specific mode with either constant speed or acceleration is not robust for random moving) [25]. When the target track starts from $(\varphi(t_0), d_0)$ and arrive at $(\varphi(t_1), d_1)$, the AoA $\theta(t)$ can be expressed as follow

$$\theta(t) = \theta_0 + \int_{t_0}^{t} \omega_m(t)dt. \tag{14}$$

Thus, the distance vector can be modeled with the time-frequency features and expressed as

$$\Delta\mathbf{d}(\theta(t)) = \begin{bmatrix} 2r\sin(\frac{\alpha_{t_2}}{2})\sin\left(\theta(t_1) - \frac{\alpha_{t_2}}{2}\right) \\ 2r\sin(\frac{\alpha_{t_3}}{2})\sin\left(\theta(t_2) - \frac{\alpha_{t_3}}{2}\right) \\ \cdots \\ 2r\sin(\frac{\alpha_{t_n}}{2})\sin\left(\theta(t_n) - \frac{\alpha_{t_n}}{2}\right) \end{bmatrix}. \tag{15}$$

Correspondingly, the real-time AoA is estimated by

$$\min_{\theta_{t_0}, b} \quad h(\theta_{t_0}, b) = \|\widetilde{\Delta\mathbf{d}} - \Delta\mathbf{d}(\theta(t), b)\|. \tag{16}$$

Obviously, this objective function optimization is similar to the static AoA calculation. Thus, we estimate $\theta(t)$ based on the iterative method in Section IV-A and design the tracking algorithm as illustrated in Algorithm 1. To track a moving target, the robot estimates its relative real-time location and schedules the path to move to the destination. Specifically, the mobile anchor keeps sending the ranging requests and measuring the rotation angle in the tracking. The ranging difference $\Delta d(t)$ and the corresponding angle $\varphi(t)$ are recorded in a measurement queue. As the target may move in the tracking, the target speeds are first estimated via the Doppler shift. Further, the real-time AoA is calculated in the stochastic gradient descent optimization, during which the m random samples from the results are selected in each iteration until the error is less than the threshold or the iteration is finished. When the real-time AoA is calculated, the robot selects a reachable path to follow the moving target's location.

V. IMPLEMENTATION

As shown in Fig. 10, we implement a prototype of LTrack consisting of three components, including a tag, an anchor, and a firmware for the commercial mobile robot. The tag can be attached to static or moving objects. The anchor contains a circular antenna array that is installed on the robot. The architecture of the firmware is shown in Fig. 10(b). When the anchor needs to track the target, the result is sent to the robot controller via a wireless serial port for the target tracking. We develop the tracking firmware on the robot controller platform (Linux-armv7hf) to listen for the ranging result and calculate the destination location. The robot keeps tracking and selects a new path to move to the target when the result is updated.

Tag: The LTrack tag needs to be attached to the tracking objects and only sizes $4\,\mathrm{cm} \times 10\,\mathrm{cm}$ because it only has essential
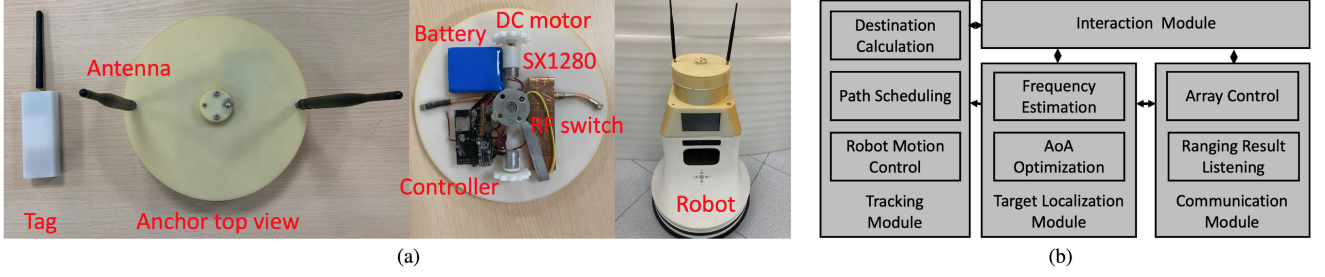
Fig. 10. Hardware implementation and firmware design of the LTrack system on a robot. (a) Hardware implementation. (b) Firmware framework.

Algorithm 1: Tracking Optimization.

Input: maximum times of iteration $iter_{max}$, iterative threshold τ, the step size μ, the distance threshold d.
Output: the target node location $\tilde{p}$
Start rotating the antenna array and record its orientation $\alpha_g(t)$, its rotation speed $\omega_g(t)$, the robot location p_r, the robot orientation φ_r, and the robot rotation speed ω_r;
Initialize iterative error $e_{iter} = \tau$, $\theta = \theta_0, b = b_0$;
while $d_t \leq d$ **do**
    Initialize $iter = 0$;
    Collect new ranging result $\Delta d(t)$;
    Calculate $\theta(t)$ via (13) and (14);
    while $iter \leq iter_{max}$ **do**
        Select m samples θ_m Δd_m random from the results;
        Calculate $h_t = h(\theta, b)$ via (16);
        Update θ and b via (10);
        if $h_t - h_{t+1} \leq \tau$ **then**
            $\theta = \theta_{t+1}$;
            $b = b_{t+1}$;
            break ;
        end
        $h_{t+1} = h_t$;
        $iter = iter + 1$;
    end
    Calculate the target relative location $\tilde{p}$ via (θ, d) and move to this destination;
end
return $\tilde{p}$;

---

components for communication and tracking. We simplify the hardware design to save power and extend battery life. The tag uses an ultra-low-power microcontroller STM32L476 and an SX1280 LoRa chip. The tag transmits and receives messages or responses to ranging packets sent by the anchor. Note that our design is compatible with the standard frequency hopping protocol. Thus, any devices that support 2.4 GHz LoRa ranging can serve as the tag. We choose SX1280 to prototype our system due to its wide availability. The cost of an LTrack tag is about 12 US$.

Anchor: The LTrack anchor runs the proposed ranging tasks and coordinates with the robot through wireless serial ports. The anchor is equipped with a circular antenna array with two omnidirectional antennas. Following the design in Section IV-A1, the two antennas are separated by 0.2 m. We connect the two antennas to an HMC241 RF switch to multiplex the single RF channel of the SX1280 LoRa chip. We install those components on a rotary board that is driven by a DC motor. The angle of rotation is recorded via a photoelectric rotary encoder. The speed of rotation is controlled by a PID controller that drives the DC motor with pulse-width modulation. The cost of an LTrack anchor is about 20 US$.

Robot firmware: To apply the LTrack system on a real robot, we develop a new robot firmware. As illustrated in Fig. 10(b), the firmware has a communication module, a target localization module, a tracking module, and an interaction module. The communication module bridges the LTrack anchor and the robot controller via wireless serial ports. The target location module performs real-time AoA and frequency estimations and sends the results along with the ToF estimation results to the tracking model. The tracking module fuses the results and schedules the tracking path. The interaction process the voice command from the user to identify which LTrack tag to track. In our settings, the firmware is running on a Khadas VIM3 single-board computer, which belongs to the commercial robot.

VI. EVALUATION

In this section, we conduct practical experiments in complex indoor environments to evaluate the performance of LTrack system. We also demonstrate the deployability of our system in a large indoor space through simulations.

A. Indoor Experiments

We first evaluate the AoA estimation accuracy in LOS and NLOS scenarios, and then the overall tracking performance in different environments with the prototype described in Section V.

1) LOS AoA Estimation:

a) Setup: The bandwidth and the spreading factor of the LoRa are set to 1625 kHz and SF5, respectively. The transmitting power of the tag and the anchor is 12.5 dBm. The rotation speed of the circular antenna array is 40 degree/s. We place the LTrack tag away from the LTrack anchor at different distances, i.e, 40 m, 50 m, and 60 m. As shown in Fig. 12, the anchor is placed on a
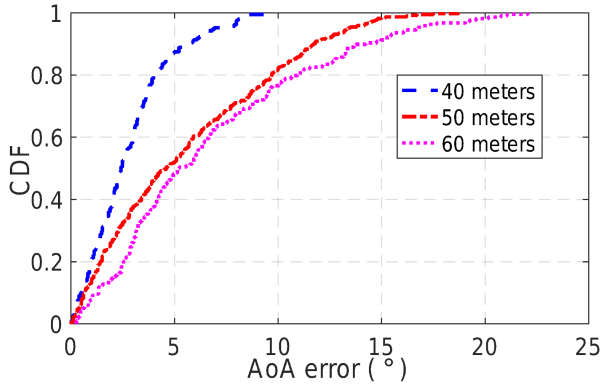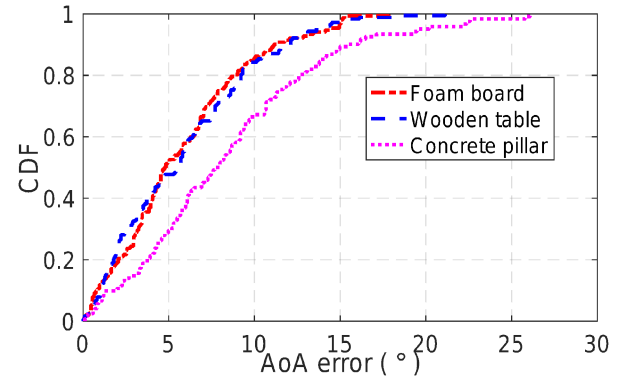
Fig. 11. LOS AoA estimation errors in different ranges.

Fig. 12. LOS and NLOS AoA estimations.

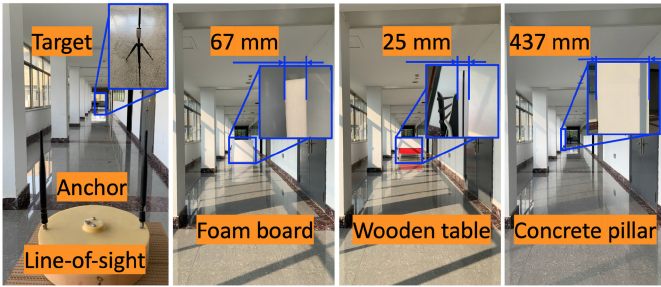Fig. 13. NLOS AoA estimation error with blockage of different obstacles 50 m away from the anchor.

Fig. 14. The tracking experiment in an indoor lab space. The robot begins tracking at (0,0) and finishes at (3.8,10).

tripod at the same height as the target and starts the estimation from different orientations. For each distance setting, we let the anchor estimate the AoA of the tag 200 times.

b) Results: Fig. 11 shows the CDF of AoA estimation error when tracking the tag located at different distances with LOS. The LTrack anchor is able to track the tag with a median error of 2.4 degrees when they are 40 m apart from each other. The LTrack achieve AoA estimation errors of 4.5 degrees at 50 m, and 5.2 degrees at 60 m. We can see that AoA estimation error increases with distance. This is because the signal attenuates after the long-distance propagation. We also notice that the estimation accuracy is similar at 50 m and 60 m, where their median errors differ by 0.7 degrees. In particular, near 85% of estimation errors are less than 5 degrees at 40 m. The 5 degrees AoA error can be translated into a 3.5 m (40 m * tan5°) distance from the actual location of the tag. The performance will improve as the robot moves towards the target, and thus has a shorter distance.

2) NLOS AoA Estimation:

a) Setup: When the robot is tracking an object, the signal path between the anchor and the tag may be NLOS. Thus, we place the tag behind the obstacle to block the signal path. As shown in Fig. 12, we use three kinds of obstacles to create NLOS scenarios, including a foam board, a wooden table, and a concrete pillar. The distance between the anchor and the tag is 50 m. For each type of obstacle, we perform the AoA estimation 200 times. The parameters of LoRa radio are the same with Section VI-A1.

b) Results: Fig. 13 presents the CDF of AoA estimation error when different types of obstacles block the signal path.
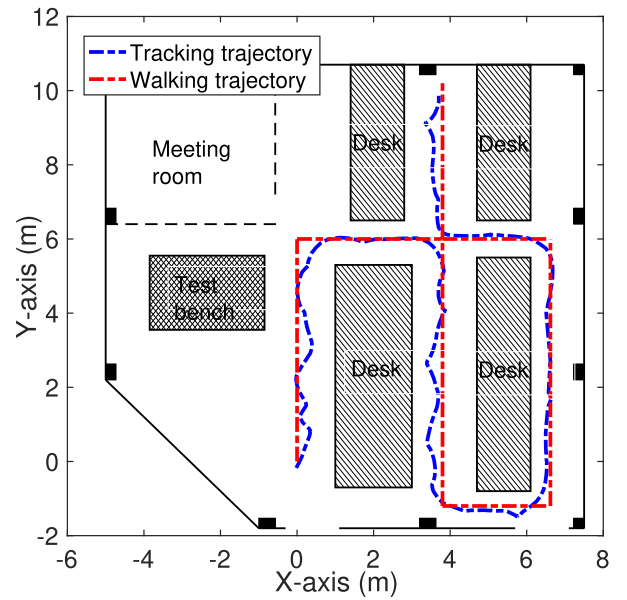
LTrack respectively achieves a median AoA estimation error of 5.72 degrees, 5.83 degrees, and 8.49 degrees, with the blockage of the foam board, wooden table, and concrete pillar. Compared with the LOS scenario, the performance of AoA estimation degrades in NLOS settings. The NLOS results meet our expectations because the signal attenuates significantly due to reflections, scattering, and diffraction. We find that the foam and wooden obstacles have fewer negative impacts on the AoA estimation performance because the LoRa signal can easily penetrate these obstacles. Nevertheless, the performance degradation caused by NLOS paths can be mitigated by the fact that the direct signal path between the anchor and the tag changes with the robot's movement.

3) Tracking in a Lab Space:

a) Setup: We evaluate the tracking performance of LTrack in a 137 m² lab space. Fig. 14 shows the floor plan of the lab. The lab has a smart manufacturing testbed with many metal devices
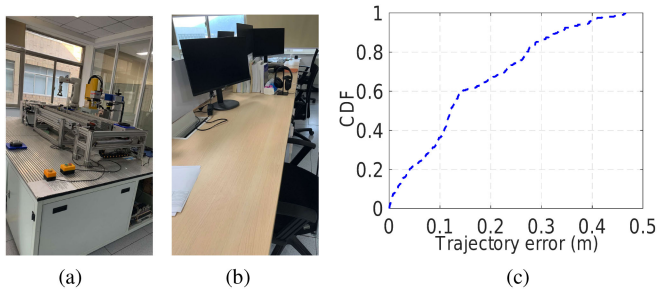
Fig. 15. Obstacles in the lab and the tracking error. (a) Test bench. (b) Desk. (c) CDF of the tracking error.
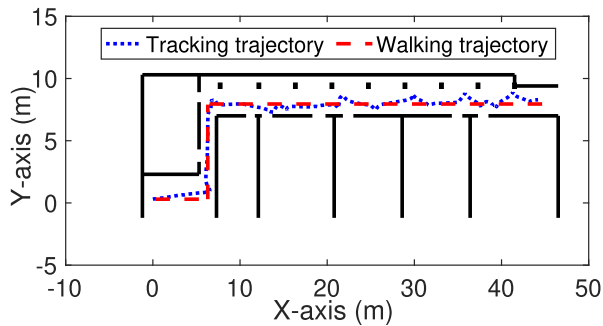

Fig. 17. Tracking experiment in a corridor. A person holds the tag in nature and walks at a speed of 0.5 m/s.

Fig. 16. Tracking experiment in a corridor. A person holds the tag in nature and walks at a speed of 0.3 m/s.

Fig. 18. Tracking errors with different walking speeds.

Fig. 19. Tracking performance comparison with the popular systems ITrackU [26] and BLoc [27].

(e.g., robot arms) and many desks with PC or personal staff on them, as shown in Fig. 15(a) and Fig. 15(b), respectively. The user holds the LTrack tag in hand and walks naturally along a preset path, which has been marked in red in Fig. 14. The anchor and the robot estimate the tag location to follow the user. The parameters of LoRa radio are consistent with Section VI-A1.

b) Results: The dashed blue line in Fig. 14 represents the tracking trajectory of the robot. We compute the tracking error according to the euclidean distance between the robot's tracking trajectory and the ground truth. Fig. 15(c) presents the CDF of the tracking error. The LTrack system achieves a median error of 0.12 m and an 80 percentile error of 0.27 m. During the tracking, we set a safe distance (i.e., 1 to 2 m) between the target and the robot as the robot may deviate from the ground-truth trajectory.

4) Tracking in a Corridor:

a) Setup: We further conduct tracking experiments in a corridor sized $10 \times 60\,\text{m}^2$. Fig. 16 shows the floor plan of the corridor. There are many concrete pillars in the corridor. We adopt the same setting in Section VI-A3, except the user walking speed. The user walks along the corridor at speeds of 0.3 m/s and 0.5 m/s.

b) Results: Fig. 16 and Fig. 17 illustrate the tracking results at different user walking speeds. Fig. 18 presents the CDFs of the tracking errors. We can see that the tracking error increases when the user walks at a faster speed. LTrack estimates the tag's velocity based on discretely collected samples at a certain frequency instead of continuously sampling. The discrete sampling cannot capture some motion features when the tracking target moves rapidly. The LTrack system still achieves sub-meter tracking
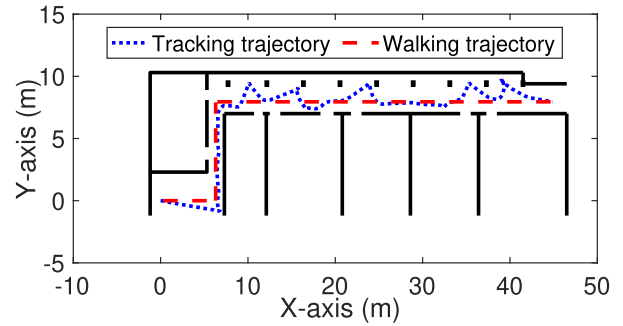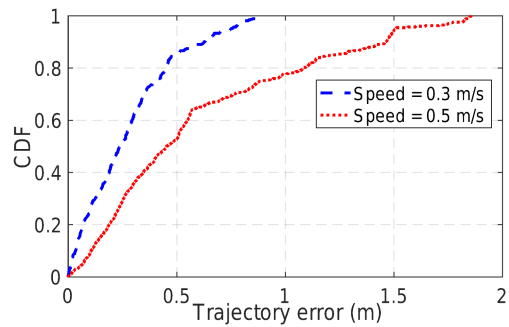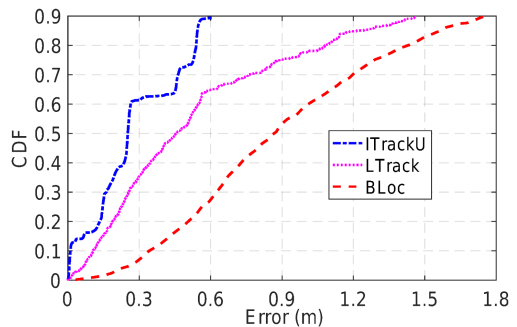
accuracy. The median errors at the speed of 0.3 m/s and 0.5 m/s are 0.24 m and 0.45 m, respectively.

5) Tracking Performance Comparison:

a) Setup: We compare the indoor tracking performance with the popular UWB-based tracking system, ITrackU [26], and the Bluetooth-based system, BLoc [27].

b) Results: The results are illustrated in Fig. 19. The ITrackU system achieves an accurate tracking performance with 80% errors less than 0.6 m. The high ToF resolution of UWB improves the ranging performance and further derives better tracking accuracy. However, the coverage of ITrackU is limited due to its fast attenuation. In ITrackU, the experiment is conducted in a $2.4 \times 1.7\,\text{m}^2$ area. Compared with the BLoc system, LTrack is more accurate due to our efficient optimization in LoRa AoA estimation.
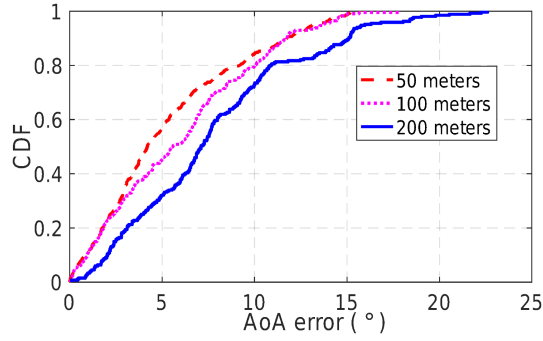
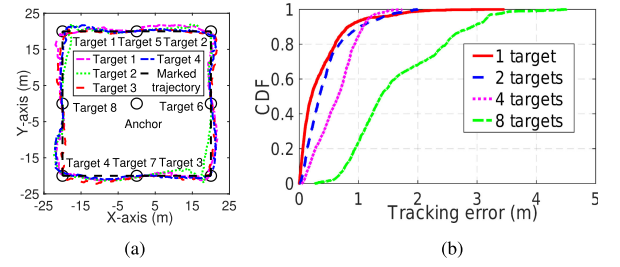Fig. 20. LTrack AoA estimation performance at different ranges.

Fig. 21. Multiple target tracking in one anchor. (a) Multiple target tracking. (b) CDF of the tracking error.
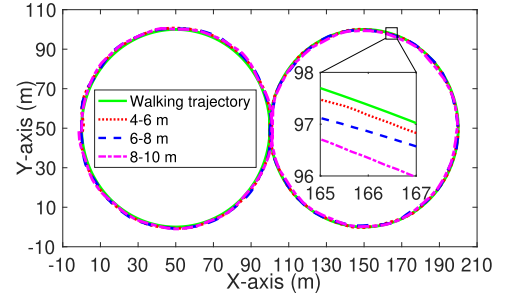

Fig. 22. Tracking simulation in a large indoor space with different safe distance settings.
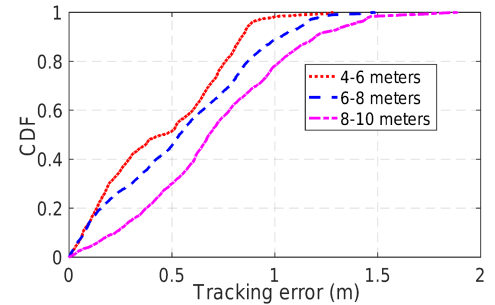

Fig. 23. Tracking errors with different safe distance settings.

B. Deployability Investigation

Based on our system model and data traces retrieved from experiments in Section VI-A, we investigate the deployability of the LTrack via simulations. We model the signal quality based on real RSSI measurements at different distances. The path-loss model is fitted as $RSSI_d = -28.31 * log10(d) - 26.96$. Further, the SNR is derived from the RSSI as $SNR = RSSI - (-90)$. The antenna rotation speed and the ranging period are the same as experiments before.

1) Distance: The LoRa signal attenuates with distance, which impacts the performance of the AoA estimation. To understand how distance affects the AoA estimation accuracy, we run simulations at different distances. The tag is apart from the anchor at a distance of 50 m, 100 m, and 200 m. For each distance, we collect 200 estimation values, and the CDF is illustrated in Fig. 20. The median AoA estimation errors in 50 m, 100 m, and 200 m are 4.3 degrees, 5.6 degrees, and 7.1 degrees, respectively. We find that the simulation results at 50 meters well match our experimental results. In the path-loss model, the signal attenuates slowly when the distance increases. For example, the RSSI decreases by 22 dBm when the distance changes from 10 m to 60 m. But it just attenuates 5 dBm when the distance changes from 100 m to 150 m. Thus, even the distance is 200 m, the AoA estimation median error is still less than 10 degrees, which is sufficient for the robot to move close to the target. As the robot is approaching the target, the AoA estimation accuracy increases and will be stable.

2) Scalability: To investigate the scalability of the LTrack system, we first evaluate the multiple target tracking performance. We conduct tracking simulations with the same parameters as the experiment before. The anchor is placed at the central point of a $50 \times 50 \, m^2$ area. We first track one target, and then two targets, and further four targets, and finally eight targets. The anchor sends the ranging packets to different targets in turn. The targets move at the speed of 0.5 m/s and follow the marked trajectory as illustrated in Fig. 21(a). The estimated trajectories are presented when we add four targets. These four targets start moving at the same time from different locations. When the target number is larger, we analyze the CDF of the average trajectory error as illustrated in Fig. 21(b).

The 80% errors of one target, two targets, four targets, and eight targets are 0.60 m, 0.67 m, 0.93 m, and 2.47 m, respectively.

The performance is degraded when the anchor tracks more targets simultaneously. This is because the anchor needs to send the ranging packets to each target in turn. The motion features of the target are lost during the cyclic ranging task, which prevents enough sampling. However, the eight targets average error is still less than 5 meters as the anchor estimates the AoA and the velocity of the target.

To evaluate the performance in a large area, we conduct simulations in a $100 \times 200 \, m^2$ space. As shown in Fig. 22, the target starts from the point (0, 50) with a 1 m/s moving speed. The robot may keep a safe distance between the target and itself. Thus, we let the robot track the target with a safe distance of 4-6 m, 6-8 m, and 8-10 m in three settings. Fig. 23 presents the CDF of the tracking error. The median errors of tracking distances of 4-6 m, 6-8 m, and 8-10 m are 0.45 m, 0.55 m, and 0.72 m, respectively. Although the safe distance impacts the performance, the LTrack system still achieves an 80 percentile error of 1.03 m in the 20000 m^2 indoor space. These results indicate that the LTrack

system is feasible to track a target with different safe distance requirements in a large indoor space.

VII. Related Work

Related work can be broadly categorized as follows:

LoRa localization: LoRa has been studied for both indoor and outdoor localization due to its features of low power consumption and long communication range. Recent studies have proposed multiple methodologies to exploit LoRa radios for localization, including RSSI-based (fingerprinting and path loss model) and TDoA-based. The path loss model is mainly applicable in outdoor environments. For example, the SateLoc system [28] recognizes the land-cover types on the signal paths by identifying the satellite images and achieves a median localization error of 47.1 m. However, it is challenging in the indoor environment due to signal reflections and attenuation caused by walls and other barriers. Although location fingerprinting with RSSI can achieve sub-10 m accuracy in an indoor environment, it needs a blanket process of fingerprinting at many, or even all locations. Moreover, the RSSI fingerprints face an aging issue [15]. Several studies have investigated the feasibility of adopting TDoA-based approaches to localize LoRa end devices. However, the localization accuracy is limited by the resolution in most sub-1 GHz LoRa devices.

To improve localization accuracy, researchers exploit bandwidth combination techniques to increase bandwidth. OwLL [16] aggregates TV whitespaces and ISM bands by allowing LoRa end device hopping multiple frequencies. OwLL computes the location of the end device after integrating TDoA results from multiple base stations. Besides these aforementioned works on sub-1 GHz, a study [29] shows that the new generation LoRa, which operates on 2.4 GHz bands, performs well in outdoor localization.

RF-based indoor tracking and localization: Enabling robots to track and follow objects in indoor environments is a fundamental task in robotics. Researchers have exploited various RF signals to implement the indoor tracking and localization system, including RFID, BLE, ADS-B, UWB, and Wi-Fi. These RF-based systems can be realized through a range of wireless signal characteristics, including AoA, ToF, and signal amplitude (RSSI) [30]–[32].

According to the infrastructure requirement, prior works on RF-based indoor tracking can be further divided into two categories, i.e., infrastructure-based and infrastructure-free. Infrastructure-based systems require users to set up additional devices as infrastructure. For example, using multiple Wi-Fi routers to locate a target has been studied extensively in the past two decades. The UWB-based system achieves accurate tracking performance via high resolution ToF estimation [26]. These systems achieve excellent performance with a few millimeters accuracy in localization. However, they adopt a dense deployment strategy to cover a large area and thus increase the cost to achieve such high accuracy. Moreover, users need to fine-tune the devices that severing as infrastructure, including the location, orientation, and antenna separation, which requires expertise and extra effort [31], [32].

In contrast, infrastructure-free tracking systems take advantage of easy deployment, which does not require prior deployment, or leverage existing devices, e.g., Wi-Fi APs [6], [33]–[36]. While using existing devices mitigates the cost issue, the scalability of these systems is restricted. For instance, the field hospital may not have enough time to install Wi-Fi APs in response to COVID-19 emergencies. Thus, it is desirable to have a tracking system that supports on-site deployment.

Antenna array emulation: Antenna array has been widely adopted in wireless localization due to its capability of beam steering. To reduce the number of antennas in an antenna array, researchers proposed to use SAR, which allows a single-antenna device to emulate an antenna array. In SAR, the antenna moves along a particular trajectory and takes snapshots of received signals at multiple spatial locations. Researchers have applied SAR on many RF sources for device localization, e.g., RFID [37], [38].

The most related work to ours is Ubicarse [33], which enables handheld devices to emulate antenna arrays. Ubicarse uses readers of motion sensors to recover the trajectory between two signal snapshots. Note that LTrack faces different challenges in empowering robots tracking with LoRa. First, the LoRa anchor does not provide phase information like Wi-Fi cards. Second, the relative position between the antenna and the target keeps changing in a tracking system, which causes errors in estimation.

Summary: The main task of LTrack is tracking, which is orthogonal to most localization applications. An important assumption in many LoRa localization systems is that the target is *static* or *quasi-static*. However, this assumption does not stand in a tracking system. Moreover, the resources for signal processing and data storage are unavailable or expensive on a mobile robot, making it difficult to translate the existing localization systems into tracking systems. To the best of our knowledge, LTrack is the first real-time tracking system based on LoRa.

VIII. Conclusion

This paper presented LTrack, a system that allows mobile robots to perform indoor tracking using 2.4 GHz LoRa signals without prior deployed infrastructure. LTrack enabled LoRa devices to estimate AoA and track moving objects by a set of hardware and software designs. We developed an LTrack prototype system on a mobile robot. Experiments showed that LTrack can track a moving object with decimeters level accuracy. LTrack offers an infrastructure-free, low-cost, and lightweight approach for mobile robots to track objects in the indoor environment.

References

[1] Fortune Business Insights, "Service robotics market size." Accessed: Nov., 2021. [Online]. Available: https://www.fortunebusinessinsights. com/industry-reports/service-robotics-market-101805

[2] W. Chen, J. Liu, H. Guo, and N. Kato, "Toward robust and intelligent drone swarm: Challenges and future directions," *IEEE Netw.*, vol. 34, no. 4, pp. 278–283, Jul./Aug. 2020.

[3] N. Kato *et al.*, "Location awareness system for drones flying beyond visual line of sight exploiting the 400 MHz frequency band," *IEEE Wireless Commun.*, vol. 26, no. 6, pp. 149–155, Dec. 2019.

[4] J. Suh, E. Y. Choi, and F. Borrelli, "Vision-based race track SLAM based only on lane curvature," *IEEE Trans. Veh. Technol.*, vol. 69, no. 2, pp. 1495–1504, Feb. 2020.

[5] F. Li *et al.*, "VisioMap: Lightweight 3-D scene reconstruction toward natural indoor localization," *IEEE Internet Things J.*, vol. 6, no. 5, pp. 8870–8882, Oct. 2019.

[6] S. Shi, S. Sigg, L. Chen, and Y. Ji, "Accurate location tracking from CSI-based passive device-free probabilistic fingerprinting," *IEEE Trans. Veh. Technol.*, vol. 67, no. 6, pp. 5217–5230, Jun. 2018.

[7] D. Chen, K. G. Shin, Y. Jiang, and K.-H. Kim, "Locating and tracking BLE beacons with smartphones," in *Proc. 13th Int. Conf. Emerg. Netw. Experiments Technol.*, 2017, pp. 263–275.

[8] Q. Tian, K. I.-K. Wang, and Z. Salcic, "Human body shadowing effect on UWB-based ranging system for pedestrian tracking," *IEEE Trans. Instrum. Meas.*, vol. 68, no. 10, pp. 4028–4037, Oct. 2019.

[9] M. Wang *et al.*, "Accurate and real-time 3-D tracking for the following robots by fusing vision and ultrasonar information," *IEEE/ASME Trans. Mechatronics*, vol. 23, no. 3, pp. 997–1006, Jun. 2018.

[10] C. Kumar and K. Rajawat, "Dictionary-based statistical fingerprinting for indoor localization," *IEEE Trans. Veh. Technol.*, vol. 68, no. 9, pp. 8827–8841, Sep. 2019.

[11] Y. Kawamoto, R. Sasazawa, B. Mao, and N. Kato, "Multilayer virtual cell-based resource allocation in low-power wide-area networks," *IEEE Internet Things J.*, vol. 6, no. 6, pp. 10665–10674, Dec. 2019.

[12] B. Xie and J. Xiong, "Combating interference for long range LoRA sensing," in *Proc. 18th Conf. Embedded Networked Sensor Syst.*, 2020, pp. 69–81.

[13] F. Zhang *et al.*, "Exploring LoRA for long-range through-wall sensing," *Proc. ACM Interactive, Mobile, Wearable Ubiquitous Technol.*, vol. 4, no. 2, pp. 1–27, 2020.

[14] K.-H. Lam, C.-C. Cheung, and W.-C. Lee, "RSSI-based LoRA localization systems for large-scale indoor and outdoor environments," *IEEE Trans. Veh. Technol.*, vol. 68, no. 12, pp. 11778–11791, Dec. 2019.

[15] C. Gu, L. Jiang, and R. Tan, "LoRA-based localization: Opportunities and challenges," in *Proc. Int. Conf. Embedded Wireless Syst. Netw.*, 2019, pp. 413–418.

[16] A. Bansal, A. Gadre, V. Singh, A. Rowe, B. Iannucci, and S. Kumar, "OwLL: Accurate LoRA localization using the TV whitespaces," in *Proc. 20th Int. Conf. Inf. Process. Sensor Netw.*, 2021, pp. 148–162.

[17] Z. Shi, X. Chang, C. Yang, Z. Wu, and J. Wu, "An acoustic-based surveillance system for amateur drones detection and localization," *IEEE Trans. Veh. Technol.*, vol. 69, no. 3, pp. 2731–2739, Mar. 2020.

[18] H. Huang, J. Yang, H. Huang, Y. Song, and G. Gui, "Deep learning for super-resolution channel estimation and DOA estimation based massive MIMO system," *IEEE Trans. Veh. Technol.*, vol. 67, no. 9, pp. 8549–8560, Sep. 2018.

[19] C. Zhang, F. Li, J. Luo, and Y. He, "ILocScan: Harnessing multipath for simultaneous indoor source localization and space scanning," in *Proc. 12th ACM Conf. Embedded Netw. Sensor Syst.*, 2014, pp. 91–104.

[20] F. Zhao, Z. Cao, Y. Xiao, J. Mao, and J. Yuan, "Real-time detection of fall from bed using a single depth camera," *IEEE Trans. Automat. Sci. Eng.*, vol. 16, no. 3, pp. 1018–1032, Jul. 2019.

[21] X. Gao, S. Roy, and G. Xing, "MIMO-SAR: A hierarchical high-resolution imaging algorithm for mmWave FMCW radar in autonomous driving," *IEEE Trans. Veh. Technol.*, vol. 70, no. 8, pp. 7322–7334, Aug. 2021.

[22] W. Gong and J. Liu, "RoArray: Towards more robust indoor localization using sparse recovery with commodity WiFi," *IEEE Trans. Mobile Comput.*, vol. 18, no. 6, pp. 1380–1392, Jun. 2019.

[23] X. Wang, L. Gao, S. Mao, and S. Pandey, "CSI-based fingerprinting for indoor localization: A deep learning approach," *IEEE Trans. Veh. Technol.*, vol. 66, no. 1, pp. 763–776, Jan. 2017.

[24] L. Bottou, "Large-scale machine learning with stochastic gradient descent," in *Proc. COMPSTAT*, 2010, pp. 177–186.

[25] C. Li, Z. Shi, and J. Chen, "Hardware architecture and optimisation of FPP particle PHD filter for multi-target tracking in cyber-physical systems," *IET Control Theory Appl.*, vol. 11, no. 11, pp. 1830–1837, 2017.

[26] Y. Cao, A. Dhekne, and M. Ammar, "ITrackU: Tracking a pen-like instrument via UWB-IMU fusion," in *Proc. 19th Annu. Int. Conf. Mobile Syst., Appl., Serv.*, 2021, pp. 453–466.

[27] R. Ayyalasomayajula, D. Vasisht, and D. Bharadia, "Bloc: CSI-based accurate localization for BLE tags," in *Proc. 14th Int. Conf. Emerg. Netw. Experiments Technol.*, 2018, pp. 126–138.

[28] Y. Lin, W. Dong, Y. Gao, and T. Gu, "SateLoc: A virtual fingerprinting approach to outdoor LoRA localization using satellite images," *ACM Trans. Sensor Netw.*, vol. 17, no. 4, pp. 1–28, 2021.

[29] K. Hu, Y. Chen, S. He, Z. Shi, J. Chen, and Z. Tao, "ILoc: A low-cost low-power outdoor localization system for Internet of Things," in *Proc. IEEE Glob. Commun. Conf.*, 2019, pp. 1–6.

[30] J. Wang, N. Tan, J. Luo, and S. J. Pan, "WOLoc: WiFi-only outdoor localization using crowdsensed hotspot labels," in *Proc. IEEE INFOCOM - IEEE Conf. Comput. Commun.*, 2017, pp. 1–9.

[31] R. Ayyalasomayajula *et al.*, "LocAP: Autonomous millimeter accurate mapping of wifi infrastructure," in *Proc. 17th USENIX Symp. Networked Syst. Des. Implementation*, 2020, pp. 1115–1129.

[32] X. Tong, H. Wang, X. Liu, and W. Qu, "MapFi: Autonomous mapping of Wi-Fi infrastructure for indoor localization," *IEEE Trans. Mobile Comput.*, to be published, doi: 10.1109/TMC.2021.3108155.

[33] S. Kumar, S. Gil, D. Katabi, and D. Rus, "Accurate indoor localization with zero start-up cost," in *Proc. 20th Annu. Int. Conf. Mobile Comput. Netw.*, 2014, pp. 483–494.

[34] M. Kotaru, K. Joshi, D. Bharadia, and S. Katti, "SpotFi: Decimeter level localization using WiFi," in *Proc. ACM Conf. Special Int. Group Data Commun.*, 2015, pp. 269–282.

[35] D. Vasisht, S. Kumar, and D. Katabi, "Decimeter-level localization with a single WiFi access point," in *Proc. 13th USENIX Symp. Networked Syst. Des. Implementation*, 2016, pp. 165–178.

[36] Z. Chen *et al.*, "M^3: Multipath assisted Wi-Fi localization with a single access point," *IEEE Trans. Mobile Comput.*, vol. 20, no. 2, pp. 588–602, Feb. 2021.

[37] H. Liu, Y. Ma, Y. Jiang, and C. Tian, "Crucial or unnecessary? Analysis on phase differential in holographic SAR RFID localization," *IEEE Trans. Veh. Technol.*, vol. 70, no. 2, pp. 1984–1988, Feb. 2021.

[38] J. Wang and D. Katabi, "Dude, where's my card? RFID positioning that works with multipath and non-line of sight," in *Proc. ACM SIGCOMM Conf. SIGCOMM*, 2013, pp. 51–62.

Kang Hu (Student Member, IEEE) received the B.Sc. degree from the School of Mechanical Engineering and Electronic Information, China University of Geosciences, Wuhan, China, in 2017. He is currently working toward the Ph.D. degree with the College of Control Science and Engineering, Zhejiang University, Hangzhou, China. His research interests include low-power wide-area networks and localization.
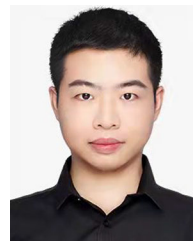
Chaojie Gu (Member, IEEE) received the Ph.D. degree in computer science and engineering from Nanyang Technological University, Singapore, in 2020. He was a Research Fellow with Singtel Cognitive and Artificial Intelligence Lab for Enterprise (SCALE) in 2021. He is currently an Assistant Professor with the College of Control Science and Engineering, Zhejiang University, Hangzhou, China. His research interests include IoT, industrial IoT, edge computing, and low power wide area networks.

Jiming Chen (Fellow, IEEE) received the Ph.D. degree in control science and engineering from Zhejiang University, Hangzhou, China, in 2005. He is currently a Professor with the Department of Control Science and Engineering, and the Vice Dean of the Faculty of Information Technology, Zhejiang University. His research interests include IoT, networked control, and cyber security.